ACS APPLIED BIO MATERIALS

www.acsabm.org Article

Modulating Fingolimod (FTY720) Anti-SARS-CoV-2 Activity Using a PLGA-Based Drug Delivery System

Renata Rank Miranda, Natália Noronha Ferreira, Edmarcia Elisa de Souza, Paula Maria Pincela Lins, Leonardo Miziara Barboza Ferreira, Arne Krüger, Valéria Maria de Oliveira Cardoso, Edison Luiz Durigon, Carsten Wrenger, and Valtencir Zucolotto*

Cite This: https://doi.org/10.1021/acsabm.2c00349 Read Online

ACCESS | Metrics & More | Article Recommendations

ABSTRACT: COVID-19 has resulted in more than 490 million people being infected worldwide, with over 6 million deaths by April 05th, 2022. Even though the development of safe vaccine options is an important step to reduce viral transmission and disease progression, COVID-19 cases will continue to occur, and for those cases, efficient treatment remains to be developed. Here, a drug repurposing strategy using nanotechnology is explored to develop a therapy for COVID-19 treatment. Nanoparticles (NPs) based on PLGA for fingolimod (FTY720) encapsulation show a size of ∼150 nm and high drug entrapment (∼90%). The NP (NP@FTY720) can control FTY720 release in a pH-dependent manner. Cytotoxicity assays using different cell lines show that NP@FTY720 displays less toxicity than the free drug. Flow cytometry and confocal microscopy reveal that NPs are actively internalized mostly through caveolin-mediated endocytosis and macropinocytosis pathways and co-localized with lysosomes. Finally, NP@FTY720 not only exhibits anti-SARS-CoV-2 activity at non-cytotoxic concentrations, but its biological potential for viral infection inhibition is nearly 70 times higher than that of free drug treatment. Based on these findings, the combination of drug repurposing and nanotechnology as NP@FTY720 is presented for the first time and represents a promising frontline in the fight against COVID-19.

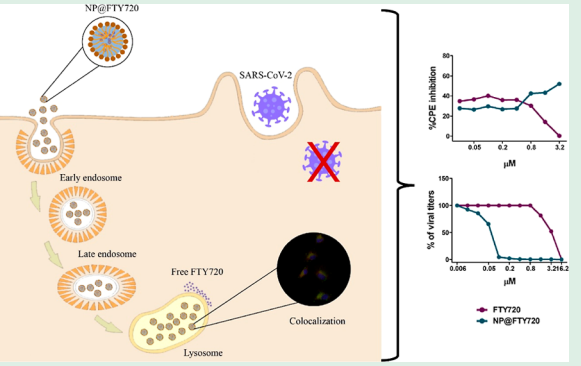

KEYWORDS: *fingolimod, FTY720, drug repurposing, nanotechnology, PLGA-based nanoparticles, antiviral activity*

1. INTRODUCTION

The emergence of pathogens presents a huge challenge to global public health.[1] Since its detection in December 2019, COVID-19, caused by severe acute respiratory syndrome coronavirus 2 (SARS-CoV-2), has resulted in more than 490 million infected people worldwide by April 05th, 2022.[2,3] Although most infected individuals are asymptomatic or experience mild cold symptoms, others may develop an exacerbated immune response, also described as a "cytokine storm," often associated with organ failure and the development of acute respiratory distress syndrome, which is usually lethal.[4,5] Consequently, over 6 million people have lost their lives due to COVID-19.

As a result of close historical, clinical, and scientific collaboration, the rapid understanding of SARS-CoV-2-host interaction and pathology allowed the development of safe vaccine options, which is an important step toward reducing viral transmission and preventing disease progression.[6,7] However, new COVID-19 cases will continue to occur, and therefore the development of effective drugs to combat the virus and/or reduce disease symptoms is urgently required to meet global demand.[8]

Although several drugs have been experimentally tested or are under clinical trials,[9−13] only a few drugs, such as the antiviral Remdesivir, the immune modulator Baricitinib, and the monoclonal antibody cocktail RegenCov, have been approved or recommended by the FDA agency to treat acute COVID-19, when hospitalization is required.[14] While the scientific community continues to search for effective molecules, according to the specific pathological features and clinical phases, different drugs including inflammation inhibitors, antiviral molecules, antirheumatic drugs, heparins, and/or hyperimmune immunoglobulins are commonly prescribed.[15] Instead of searching for a new drug agent against COVID-19, researchers and scientists have adopted a valuable, economic, fast, and efficient approach called drug repurposing,

Received: April 13, 2022
Accepted: June 12, 2022

where approved or investigational drugs are considered for a novel intervention.[16] Initial drug investigations against COVID-19 usually consisted of human clinical evidence of drug efficacy, together with *in vitro* experiments for SARS-CoV-2 and other coronaviruses. Clinical case reports indicated that multiple sclerosis (MS) patients treated with fingolimod (FTY720, Gilenya), a 2010 FDA-approved oral immunosuppressor, only developed mild COVID-19 symptoms, suggesting that this drug should be considered as a potential therapeutic candidate against SARS-CoV-2.[2,17]

FTY720 phosphate, a product of *in vivo* FTY720 phosphorylation, is a sphingosine 1 phosphate (S1P) analogue that reduces the exacerbated immune response by decreasing the T cell population of the peripheral blood.[17,18] In addition, bioactive sphingolipids played a crucial role in the regulation of viral infections, and pro-inflammatory responses were involved in the severity of COVID-19.[19] Therefore, FTY720 has recently been introduced in clinical trials to determine its role in pathology and immunomodulatory potential.[19,20]

Due to its low solubility and instability in an aqueous medium, the currently available FTY720 medicine for oral administration must be administered daily to achieve active steady-state levels in MS patients.[21,22] In addition, other therapeutic approaches for FTY720, including antitumoral activity[23] and immunosuppressants for kidney transplantation,[24] reinforced stability concerns, toxicity potential, and difficulties encountered in the maintenance of therapeutic doses.[21]

Nanotechnology and nanomedicine perform important tasks in this regard, offering not only the design of new strategies but also important improvements to ongoing treatments. It was well established that the administration of nanoencapsulated drugs facilitated effective delivery and inherent toxicity reduction. Particularly, in the case of FTY720, nanoencapsulation might provide active agent concentrations in patients' blood and tissues for a prolonged time, avoiding the necessity of repeated administrations and improving their stability in biological fluids.[24] Considering the favorable outcome of applied nanotechnology in the treatment of viral infections, diagnostic devices, and the valuable contribution of nanoscience in vaccine production,[25] it is possible to anticipate that this valuable tool will also be able to aid in COVID-19 treatment.[26] Bringing these approaches together can therefore represent a valuable strategy.

Herein, we developed a polymeric nanoparticle (NP) based on poly lactic-*co*-glycolic acid (PLGA) for encapsulating FTY720 (NP@FTY720) to investigate whether this nanosystem could improve the effect of FTY720 in terms of biosafety, release kinetics, and anti-SARS-CoV-2 properties. NP@FTY720 showed a similar cytotoxic profile to human cell lines; moreover, it led to a striking reduction in SARS-CoV-2 viral titers and cytopathic effect (CPE) in VeroCCL81 cells. Overall, we identified that the nanotechnology allied to the drug repurposing concept represents a valuable combination, and NP@FTY720 might represent a potential antiviral strategy for COVID-19 treatment.

2. EXPERIMENTAL SECTION

2.1. Preparation of NP@FTY720 by a One-Step Emulsion Solvent Evaporation Technique. NP@FTY720 was produced by the single emulsion method with modifications.[27] Briefly, 1 mg of FTY720 hydrochloride CRS (European Pharmacopoeia reference standard) and 10 mg of PLGA 85:15 (Lactel Biodegradable Polymers) were dissolved in 100 μL of ethanol and 1.4 mL of dichloromethane, resulting in a homogeneous organic phase. This phase was added to the aqueous solution of Pluronic 127 (15 mg/mL) using a syringe (5 mL) coupled to a 0.70 × 30 mm BD needle. Emulsification was carried out by 1.5 min sonication (Branson Digital Sonifier, Mexico) applying a pulse mode of 1 min on and 30 s off, with 20% amplitude in an ice bath. The resulting emulsion was evaporated under magnetic stirring to remove the organic solvent. Afterward, NPs were washed using Amicon 100 kDa cut off and stored for further characterization. Empty NPs (without FTY720) were produced following the procedure described above for comparative purposes. For internalization studies, 2 mg/mL of 3,3′-dioctadecyloxacarbocyanine perchlorate solution (DiO, Sigma-Aldrich) in ethanol (10 μL) was added to the organic phase before the sonication procedure. Afterward, the formulation was centrifuged at 10 000*g* for 10 min (Eppendorf centrifuge 5804R, Germany). NPs were further redispersed in phosphate-buffered saline (PBS) 1× and dialyzed overnight using dialysis tubing cellulose, with a 12 kDa cut off (Sigma-Aldrich, USA).

2.2. Determination of Drug Encapsulation Efficiency (EE %). FTY720 quantification was performed by applying an indirect method considering the amount of non-entrapped FTY720 (free in the supernatant) according to eq 1. To this end, NPs were placed in an Amicon 100 kDa cut off and centrifuged (5000 rpm at 25 °C, 10 min), and the solution deposited on the bottom compartment was used for EE % evaluation

$$\text{EE \%} = \frac{[]\text{FTY720 added} - []\text{non-entrapped FTY720}}{[]\text{FTY720 added}} \times 100 \quad (1)$$

The confirmation of EE % was also performed by placing a known amount of NP@FTY720 in acetonitrile for nanostructure disruption following filtration and injection in a high-performance liquid chromatographic system (HPLC). Chromatographic analyses were executed using the previously described methodology,[28] validated by us. The chromatographic HPLC system was a Waters Alliance equipment with a quaternary pump, applying a Gemini NX-C18 column (250 cm × 4.6 mm, 5 μm, 110 Å, Phenomenex) with the mobile phase acetonitrile (35:65, v/v) and triethylamine in water 0.1% (adjusted to pH 3.0 ± 0.05 with orthophosphoric acid) at a flow rate of 0.9 mL/min, and a UV detector at 220 nm. The standard analytical curve was determined by adding FTY720 (10−100 μg/mL) to the mobile phase and using the equation $y = 26701x - 8300.5$ (r^2 = 0.999). Results are shown as the mean of three independent determinations and their standard deviations (SD).

2.3. Characterization and Stability Evaluation of NPs. Particle size and the polydispersity index (PDI) were measured by dynamic light scattering (DLS) and photon correlation spectroscopy at a wavelength of 633 nm at 25 °C and a detection angle of 90°. The zeta potential (ZP) was recorded by the electrophoretic mobility at 25 °C. The analyses were carried out on Zetasizer Nano ZS (Malvern Instruments, Malvern, UK) equipment. Samples (10 μL) were diluted in 1 mL of purified water. For stability purposes, NPs were stored in a refrigerator (8 °C) and periodically (at least once a week) analyzed for size, PDI, and ZP. Results are presented as the average of three independent measurements (n = 3) and their SD.

Empty NPs and NP@FTY720 were additionally characterized for their concentration and size distribution by NP tracking analysis (NTA) in a NanoSight NS300 (Malvern Instruments, Worcestershire, UK) equipped with a sample chamber, a 532 nm laser, camera level 11/12, and 77 ± 25 particles per frame. The NPs were diluted 50× and 400× using purified water and injected into the sample chamber with a sterile 1 mL syringe. The NTA 2.3 software was used to capture images and analyze data. Videos were recorded using an EMCCD 215S camera. For internalization studies, a fluorescence filter was applied for data acquisition. All measurements were performed in triplicate, applying independent samples in duplicate, at room temperature.

Field-emission scanning electron microscopy (FEG-SEM) analyses were conducted for empty NPs and NP@FTY720 to analyze size and

https://doi.org/10.1021/acsabm.2c00349
ACS Appl. Bio Mater. XXXX, XXX, XXX−XXX

morphology. Samples were diluted (2:100 v/v) in ultrapure water, placed on a metallic holder, and left to dry at room temperature. Afterward, samples were coated with carbon, and photomicrographs were taken at different magnifications using a JEOL-JSM-7500F coupled to the Joel Pc-100 ver.2.1.0.3. Software.

2.4. *In Vitro* Release Study. Release studies of free FTY720 and NP@FTY720 were performed according to a methodology previously proposed with modifications.[29,30] A known amount of FTY720, solution, and NP@FTY720 were added to a 2 mL tube containing phosphate buffer at pH 7.4 with 0.2% of sodium lauryl sulfate (LSS) and acetate media at pH 5.0 at 37 ± 0.5 °C with 300 rpm stirring. The solubility of the FTY720 drug in both selected receptor media was previously evaluated to assure *sink* conditions. Afterward, at predetermined times (0.5, 2, 4, 8, and 24 h), the content was filtered (Amicon Ultra 30K) to isolate the released drug, and quantification was performed using the HPLC system with standard analytical curve FTY720 (10−100 μg/mL) built-in phosphate buffer pH 7.4 with 0.2% LSS (y = 4196.6x + 81 754) and acetate medium pH 5.0 (y = 2158.7x + 163 173).

Mathematical modeling with different kinetic models (Korsmeyer−Peppas, Higuchi, first order, Hixson−Crowell, Baker−Lonsdale, and Weibull) has been performed to better understand the FTY720 release kinetic from NPs using the SigmaPlot 10.0 software.

2.5. Cell Lines and Cell Culture. The cell lines used in this study were obtained from the Rio de Janeiro Cell Bank, Brazil. Immortalized human hepatocytes (HepaRG), human alveolar adenocarcinoma (A549), and kidney epithelial cells from an African green monkey (VeroCCL81) cells were used to investigate the cytotoxic potential of FTY720 and NP@FTY720; VeroCCL81 cells were further used to access the internalization mechanisms and antiviral potential of FTY720 and NP@FTY720. Cells were grown as a monolayer using Dulbecco's modified Eagle's medium (DMEM) supplemented with 10% fetal bovine serum in a humidified incubator at 37 °C with a 5% CO_2 atmosphere.

For the experiments, cells were seeded onto 96 (cytotoxicity and CPE inhibition assay) or 12 (NP internalization assay) well plates, in fresh DMEM with 10% FBS and allowed to adhere for 24 h at 37 °C with 5% CO_2. Three independent experiments (with three replicates each, for cytotoxicity and the CPE assay) were performed.

2.6. Cytotoxicity Profile. To investigate the cytotoxic profile of FTY720, NP@FTY720, and empty NPs, cells were first incubated with different concentrations of the drug and NPs for 24 and 48 h in fresh DMEM with 2.5% FBS. VeroCCL81 cells were also incubated with the test compounds for 72 h, considering the experiments with the SARS-CoV-2 virus, which were carried out for 72 h. The following control groups were kept in parallel: cells incubated with complete medium only and cells incubated with equivalent amounts of ethanol or water present in FTY720 and NP@FTY720-test groups, respectively. At the end of each exposure period, the culture medium was replaced by a fresh complete medium containing 3-(4,5-dimethylthiazol-2-yl)-2,5-diphenyltetrazolium bromide (MTT, Sigma-Aldrich) at 0.5 mg/mL. Cells were incubated for 1 h and washed with PBS, and formazan was solubilized with dimethyl sulfoxide (200 μL). The absorbance was measured at 570 m using a microplate spectrophotometer, SpectraMax M2E (Molecular Device, Inc.).

2.7. NP@FTY720 Cellular Internalization. To assess NP@FTY720 internalization kinetics, VeroCCL81 cells were incubated with NP@FTY720-DiO at 5 × 10^9 particles/mL for 0.5, 1, 2, and 4 h. Then, cells were washed three times with PBS buffer at 4 °C, harvested (0.25% trypsin, 0.02% EDTA in PBS, pH 7.2), and pelleted in a complete culture medium (1000g, 5 min). Subsequently, pellets were resuspended and washed twice by centrifugation (500g for 10 min, 4 °C) with a 0.5% BSA-Isoton solution. The fluorescence intensity of NP@FTY720-DiO was quantified in each sample by flow cytometry using FACS Calibur (BD Biosciences). Cells in complete medium and cells with the addition of non-fluorescent NP@FTY720 were used as controls. Three independent biological replicates were performed, data were processed using FlowJo software, and statistical analysis was performed using GraphPad Prism software version 8.0 (GraphPad Software Inc.).

NP@FTY720-DiO internalization in VeroCCL81 cells was further confirmed by confocal microscopy. Cells were grown on coverslips in 12-well plates and incubated with 5 × 10^9 particles/mL for 4 h. 30 minutes before finishing the treatment, 1 μM of the LysoTracker (Thermo Fisher) fluorescent probe was added to the wells to stain the lysosomes. At the end of the incubation period, cells were rinsed three times with PBS, fixed with 3.7% paraformaldehyde for 10 min, and washed three times with PBS. After blocking with 3% BSA for 1 h, the cells were rewashed with PBS, the nuclei were stained with 4′,6′-diamino-2-fenil-indol (1 μg/mL), and the coverslips were mounted with Fluoroshield medium. Cells were imaged in 1.47 μm thick z-sections using a Zeiss LSM900 laser-scanning confocal microscope (Germany). For co-localization studies, the stack of 10 cells was analyzed individually using the JACoP plugin in Fiji software, and the Pearson's coefficient was evaluated.

To investigate the endocytosis pathways involved in NP@FTY720 uptake, VeroCCL81 cells were seeded in 12-well plates and pre-incubated with different pharmacological inhibitors for 30 min at 37 °C and 5% CO_2 (amiloride 100 μg/mL, nystatin 40 μg/mL, nocodazole 5 μg/mL, dynasore 100 μg/mL, and dansyl-cadaverine 100 μg/mL). These inhibitors were chosen due to their ability to selectively inhibit different endocytosis pathways: amiloride blocks macropinocytosis, nystatin inhibits caveolae-mediated endocytosis, nocodazole interferes with microtubule-dependent uptake, hydroxyl-dynasore inhibits dynamin-mediated endocytosis, and cadaverine blocks clathrin/dynamin-dependent cell internalization. Following the pre-treatment, cells were incubated with the inhibitors and NP@FTY720-DiO at 5 × 10^9 particles/mL for 4 h. Then, cells were thoroughly washed with PBS (three times), harvested (0.25% trypsin, 0.02% EDTA in PBS, pH 7.2), and pelleted in a complete culture medium (1000g for 5 min). Subsequently, the samples were processed for flow cytometry analysis as described previously.

2.8. Viral Infection and Drug Treatment. VeroCCL81 cells seeded onto 96-well plates were pre-treated with twofold serial dilutions of FTY720, NP@FTY720, or empty NPs in fresh DMEM with 2.5% FBS. After 4 h of incubation, the SARS-CoV-2 strain[31] was diluted in DMEM with 2.5% FBS, and the cells were inoculated with the virus at a 0.1 multiplicity of infection to allow absorption for 1 h. The viral inoculum was removed, and fresh DMEM with 2.5% FBS containing twofold serial dilutions of the FTY720, NP@FTY720, or empty NPs were added back to the wells. Cells were incubated for further 72 h post-infection to assess CPE via the CellTiter-Glo (CTG) assay or for viral RNA analysis. All SARS-CoV-2 infections were performed in the BSL3 facility at the Department of Parasitology, Institute of Biomedical Sciences, University of São Paulo, Brazil.

2.9. CPE Quantification. When the CPE occurs due to viral infection, ATP depletion can be measured and correlated with the viral burden.[32,33] The inhibition of CPE following 72 h post-infection in the presence of FTY720, NP@FTY720, or empty NPs was determined via the CTG luminescent cell viability assay (Promega), following the manufacturer's instructions. A luminescent signal was recorded using a CLARIOstar multi-mode microplate reader (BMG LABTECH, Germany). Percent CPE inhibition was defined as [(test compound − virus control)/(cell control − virus control)] × 100.[32]

2.10. RNA Extraction and RT-qPCR. The viral RNA was purified using the MagMAX viral/pathogen nucleic acid isolation kit (Thermo Fisher Scientific). The samples were processed in a semiautomated NucliSens easyMAG platform (bioMérieux, Lyon, France), following the manufacturer's instructions. The detection of viral RNA was carried out on a QuantStudio 3 Real-Time PCR system (Thermo Fisher Scientific) using the AgPath-ID One-step RT-PCR kit (Thermo Fisher Scientific) and a sequence of primers and probe for the E gene.[34] The viral titers were calculated using a standard curve generated with serial dilutions of a template of known concentration and expressed in a tissue culture infectious dose (TCID50)/mL. IC_{50} values were calculated by nonlinear regression analysis using GraphPad Prism version 8.00 (GraphPad Software Inc).

https://doi.org/10.1021/acsabm.2c00349
ACS Appl. Bio Mater. XXXX, XXX, XXX−XXX

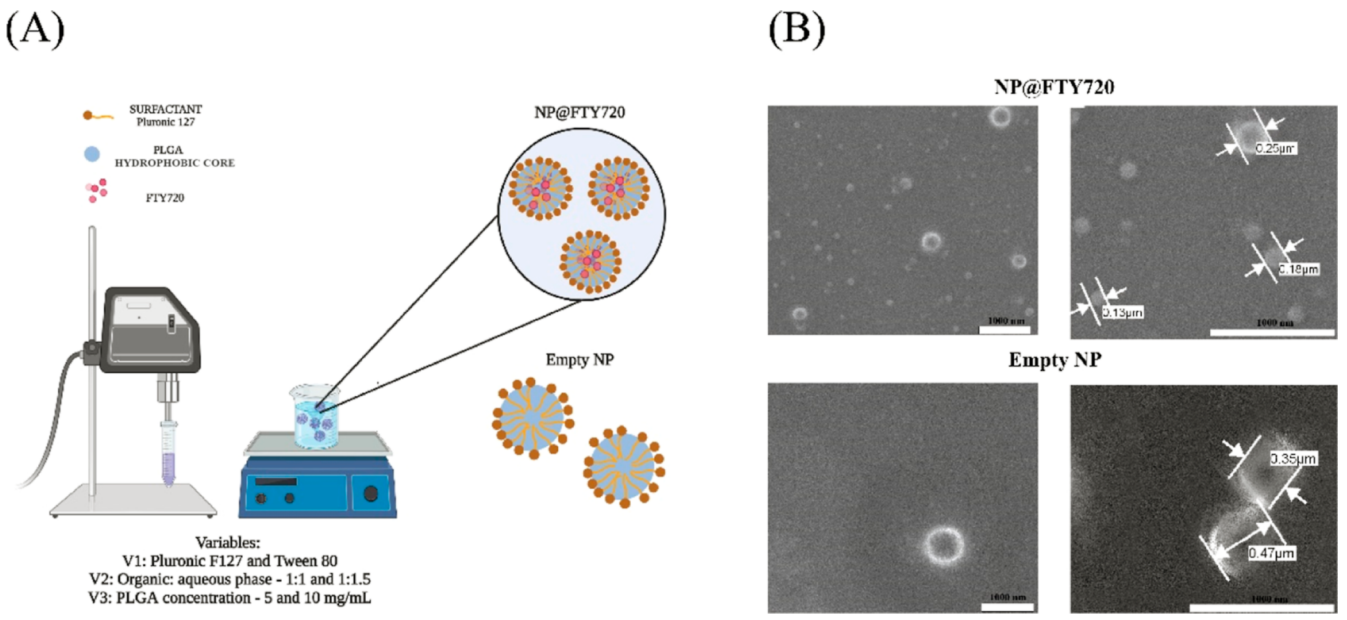

Figure 1. NP@FTY720 design and morphology. (A) Schematic illustration of NP@FTY720 preparation using a single emulsion solvent evaporation technique. (B) FEG-SEM images of empty NPs and NP@FTY720.

Table 1. Characterization of the Developed Nanostructures: Size, PDI, and ZP Data from DLS Analysis; Mean and Particle Concentration from NTA of the Synthesized Empty NPs, NP@FTY720, and NP@FTY720-DiO[a]

Samples	Dynamic Light Scattering (DLS)			Nanoparticle tracking analysis (NTA)	
	Mean Size (nm)	PDI	Zeta Potential (mV)	Mean Size (nm)	Concentration (particles/mL)
Empty NP	460±30	0.45±0.02	-17±4	294±10	6.10^10±4.10^9
NP@FTY720	149±11	0.13±0.02	14±2	181±44	7.10^11±6.10^10
NP@FTY720 -DiO	n/d	n/d	n/d	170±30	5.10^11±3.10^9

[a]Data represent the average of at least three measurements (n = 3) and SD. **I** Vertical bars indicate statistical significance ($P \geq 0.05$).

Data were obtained from four replicates (n = 4) in two biological experiments. Samples deemed to be technical failures or extreme outliers were removed.

2.11. Statistical Analysis. Statistical analysis between groups was compared using one-way analysis of variance followed by the Tukey or Dunnett post hoc test using GraphPad Prism software version 8.0 (GraphPad Software Inc.). IC_{50} values were calculated by nonlinear regression analysis using GraphPad Prism version 8.00 (GraphPad Software Inc.). Results were shown as mean ± SD for at least three independent assays (n = 3). $P < 0.05$ was selected for statistically significant differences.

3. RESULTS AND DISCUSSION

3.1. NP@FTY720 Synthesis and Characterization. Given the enormous time consumption, substantial investments, and high risk of failure involved in the process of developing a new drug, the drug repurposing approach has been increasingly applied to treat different diseases.[16,35] In addition, recent developments in nanotechnology have allowed new approaches in the field of effective drug delivery, bringing different gains in terms of therapeutic efficiency.[24] Taken together, these approaches may represent a valuable strategy for the treatment of COVID-19.

Considering the well-described and attractive properties such as biodegradability and biocompatibility, their versatility, and approval from important agencies such as the FDA and the EMA for drug delivery development intended for parenteral administration, well-established methods for NP production with high hydrophobic drug entrapment, their protective effects from drug degradation or fast release, or even the possibility to target NPs to a specific site of action,[27,36] PLGA polymer was chosen to produce polymeric NPs for FTY720 encapsulation. In the initial synthesis steps of NP@FTY720, different surfactants, such as polyvinyl alcohol, Tween 80, Pluronic F127, and Pluronic F68, were evaluated. For this selection, visual inspection prioritized the formation of a colloidal milky solution with no polymer aggregation. Thereafter, Pluronic F127 and Tween 80 were selected for further studies where parameters such as PLGA concentration (5 and 10 mg/mL) and aqueous to organic solvent ratios (1:1 and 1:1.5) were investigated using design of experiment tools. The investigated selected parameters (schematic illustration in

https://doi.org/10.1021/acsabm.2c00349
ACS Appl. Bio Mater. XXXX, XXX, XXX−XXX

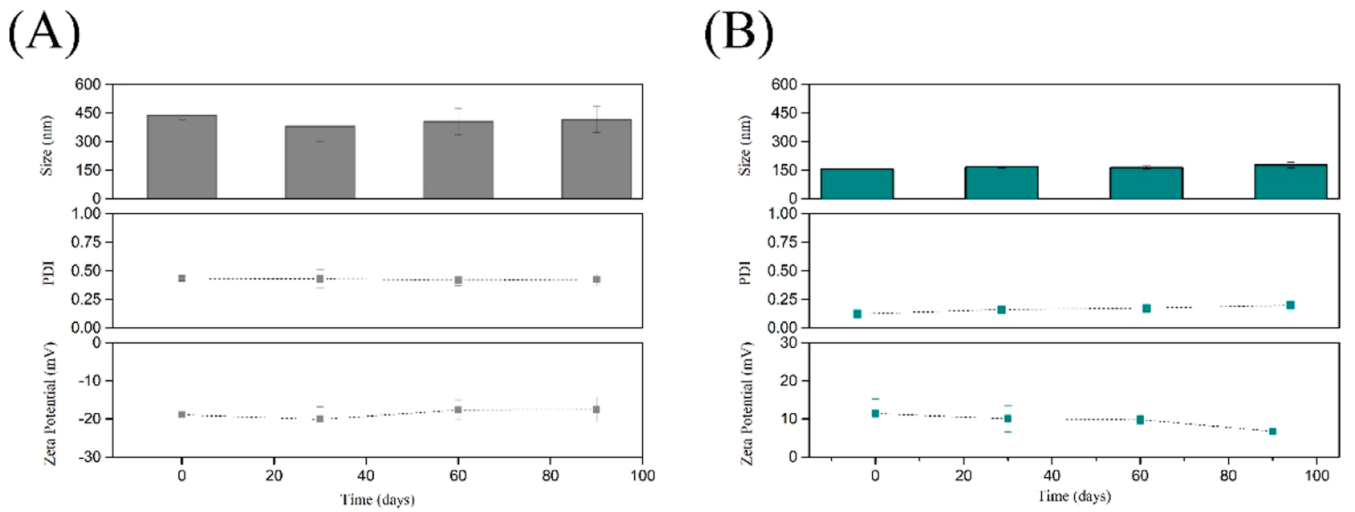

Figure 2. Long-term stability of the developed nanosystems in terms of size (nm), PDI, and ZP (mV). (A) Empty NPs and (B) NP@FTY720. Differences over time were considered statistically significant $P < 0.05$ (**).

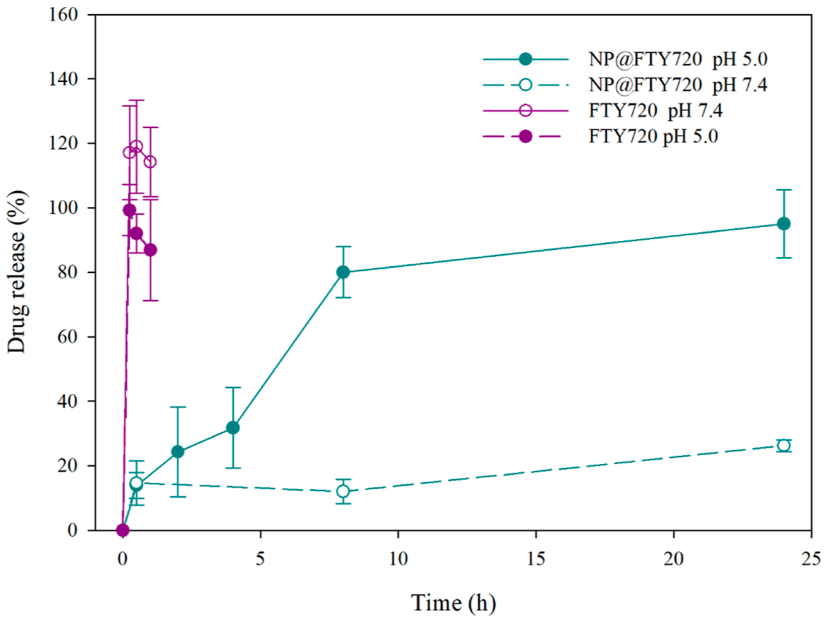

Figure 3. FTY720 release from the nanostructure system. FTY720 release profile from NP@FTY720 in a phosphate buffer with pH = 7.4 and an acetate medium with pH = 5.0. Data show the average of three independent measurements ($n = 3$) ± SD.

Figure 1A) did not significantly affect the synthesis of NP@FTY720 in terms of size, PDI, and ZP ($P \leq 0.05$). Therefore, NPs were produced using the surfactant Pluronic 127, 10 mg of PLGA, and an aqueous to organic solvent ratio of 1:1.5.

FEG-SEM images (Figure 1B) revealed spherical NPs with a size of ∼400 and ∼190 nm for empty NPs and NP@FTY720, respectively. In addition, these images expose a lower concentration of NPs for empty NPs instead of NP@FTY720.

The characterizations of NP@FTY720, empty NPs, and NP@FTY720-DiO are shown in Table 1. Particle size measurements from the DLS analysis showed values of approximately 460 nm for empty NPs and 150 nm for NP@FTY720. The PDI data revealed greater dispersity for empty NPs compared with NP@FTY720 ($P \geq 0.05$). In addition, ZP values disclosed potential charges with significant alteration in the presence (NP@FTY720) and absence of the drug (empty NP) ($P \geq 0.05$).

NTA data reinforced a significant difference in NPs considering the presence and absence of the drug in terms of size and concentration (Table 1). NP@FTY720-DiO has a size and concentration index similar to that found for NP@FTY720. The recorded values for particle concentration were further considered for internalization studies. Taking these results together, we can identify the presence of positively charged FTY720 during NP synthesis (developed at pH 5.5, considering drug stability under this condition), which has contributed to greater compaction of PLGA chains, which should have resulted in the formation of smaller and more homogeneous NP populations.

The drug entrapment efficiency recorded for NP@FTY720 was 89 ± 12%. The high capacity of FTY720 loading using the adopted method for polymeric or lipidic NPs has been previously highlighted.[7,37]

Considering that storage stability sometimes limits the application of nanostructured systems, it has translated into

https://doi.org/10.1021/acsabm.2c00349
ACS Appl. Bio Mater. XXXX, XXX, XXX−XXX

clinical practice. The prediction of colloidal stability of NPs over time can be anticipated to have physical-chemical changes and be associated with biological performance *in vitro*.[38] In this study, empty NPs and NP@FTY720 were monitored for a 3 month period in which size, PDI, and ZP were measured weekly (Figure 2). Our results showed no significant changes in size, PDI, and ZP of empty NPs during the analyzed period. In addition, negligible changes were recorded for NP@FTY720 in the period of 90 days in terms of size. However, after 90 days of analysis, small changes in PDI were also accompanied by a slight decrease in ZP values. Therefore, no significant changes were detected for both NPs (NP@FTY720 and empty NPs) in the analyses carried out *in vitro* for 2 months.

3.2. FTY720 Release from the Nanostructure System is pH Dependent. Drug release was estimated by applying a selected medium (phosphate buffer pH 7.4, with 0.2% of LSS, and acetate buffer pH 5.0) to mimic the *in vivo* environment and predict the expected drug behavior and release profile. These important data should be correlated with biological performance. Figure 3 depicts the FTY720 profiles of NP@FTY720 and the free drug at pH 7.4 and 5.0.

The results showed that the free drug reached 100% drug dissolution at 0.5 h, independent of the pH value. On the other hand, NP@FTY720 exhibited an initial release of approximately 10% in the first 2 h of the assay for both pH values. The initial release is normally associated with the diffusion and deposition of the surface layer of drug molecules.[30] Accordingly, these data reinforced the encapsulation index of approximately 90% of previously recorded data. Therefore, after 8 h, the drug release was close to 80% at pH 5.0 and still approximately 10% at pH 7.4. After 24 h, drug release reached 100% at pH 5.0, while only 20% was recorded at pH 7.4, which is almost five times lower than the data recorded at pH 5.0. This release profile showed the pH dependence of the drug release. Such behavior emphasizes that in the systemic circulation, the drug release can be preserved, and cell internalization contributes to the effective release and therapeutic outcome. The low release rates of FTY720 from nanostructured systems at pH 7.4 have been previously demonstrated.[21,39] In addition, the pH dependence of the FTY720 release comparing the investigated pH values of 5.0 and 7.4 from PLGA-based systems has also already been reported.[23]

For a deeper understanding of the driven drug release mechanisms from polymeric nanostructure matrices, release profiles were fitted to several commonly used empirical and semiempirical mathematical models that describe the dissolution release process (Figure 3).[40−42] The coefficients of determination (r^2) recorded from the different models are summarized in Table 2.

The results displayed in Table 2 show that FTY720 release from NP@FTY720 at pH 5.0 and pH 7.4 correlates better with the Weibull model (r^2 0.98 and 0.88, respectively). The mathematical model, first proposed by Weibull in 1951,[43] describes the cumulative drug amount in the medium at a certain time, which can be adjusted to different dissolution profiles according to eq 2 below.

$$m = 1 - \exp\left(\frac{-(t - T_i)^b}{a}\right) \quad (2)$$

Table 2. Mathematical Models Applied to Release Profiles: Coefficients Recorded by Baker and Lonsdale Higuchi, Korsmeyer−Peppas, First Order, Hixson−Crowell, and Weibull Models

		NP@FTY720	
mathematical models		pH 5.0	pH 7.4
Baker and Lonsdale	k	0.012	0.0005
	r^2	0.91	0.64
Higuchi	k	20.76	5.31
	r^2	0.91	0.63
Korsmeyer−Peppas	r^2	0.89	0.79
	n	0.48	0.17
	k	21.65	13.11
first order	r^2	0.95	0.42
	k	0.15	0.013
Hixson−Crowell	r^2	0.96	0.42
	k	0.04	0.004
Weibull	r^2	**0.98**	**0.80**
	b	16.2	11.0

where m represents the accumulated drug, a is the scale parameter that defines the time scale of the process (time dependence), T_i represents the lag time before the onset of the dissolution/release process, and b describes the shape of the dissolution curve progression.[44] Therefore, the b exponent indicates the main mechanism that drives drug transport from a polymeric matrix, such as PLGA. For b values greater than 1 ($b > 1$), drug transport is governed by a complex mechanism.

Since PLGA is considered a swellable matrix, physical and chemical processes should be related to complex drug releases. In the early stages, this phenomenon may be related to the liquid entrance into the polymer network, polymer hydration, and swelling. Such an event is followed by drug diffusion throughout the swollen matrix or even matrix erosion.[45] It is known that several PLGA-based NP release profiles of the drug are suitable for the Weibull model.[46]

3.3. Cytotoxic Profile of FTY720 and NP@FTY720. The viability of human cell lines, HepaRG and A549, after treatment with FTY720, NP@FTY720, and empty NPs were analyzed by the MTT assay. For both cell lines, free and encapsulated FTY720 induced a significant decrease in cell viability in a concentration-dependent manner (Figure 4). Furthermore, empty NPs did not cause cytotoxicity at any of the tested concentrations or incubation time points.

For HepaRG cells, NP@FTY720 was less toxic than FTY720 at both 24 and 48 h (Figure 4A,B). The half-maximum inhibitory concentration (IC_{50}) after 24 h of exposure was 8.8 μM for FTY720 and 15.6 μM for NP@FTY720; after 48 h; the IC_{50} values were 6.8 and 15 μM, respectively. At both exposure times, the IC_{50} values of NP@FTY720 were approximately twofold greater than the values recorded for the free drug. Therefore, the protective effect attributed to the encapsulation of FTY720 inside PLGA NPs was confirmed.

The cytotoxic profiles of FTY720 and NP@FTY720 in A549 cells were similar at both incubation time points. The IC_{50} values after 24 h of exposure to FTY720 and NP@FTY720 were 11 and 14.7 μM, respectively (Figure 4C). After 48 h, these values were 11 μM for FTY720 and 12.2 μM for NP@FTY720 (Figure 4D).

The cytotoxicity of FTY720 was investigated in different cancer cell lines due to its potential antitumoral activity.[47−49]

https://doi.org/10.1021/acsabm.2c00349
ACS Appl. Bio Mater. XXXX, XXX, XXX−XXX

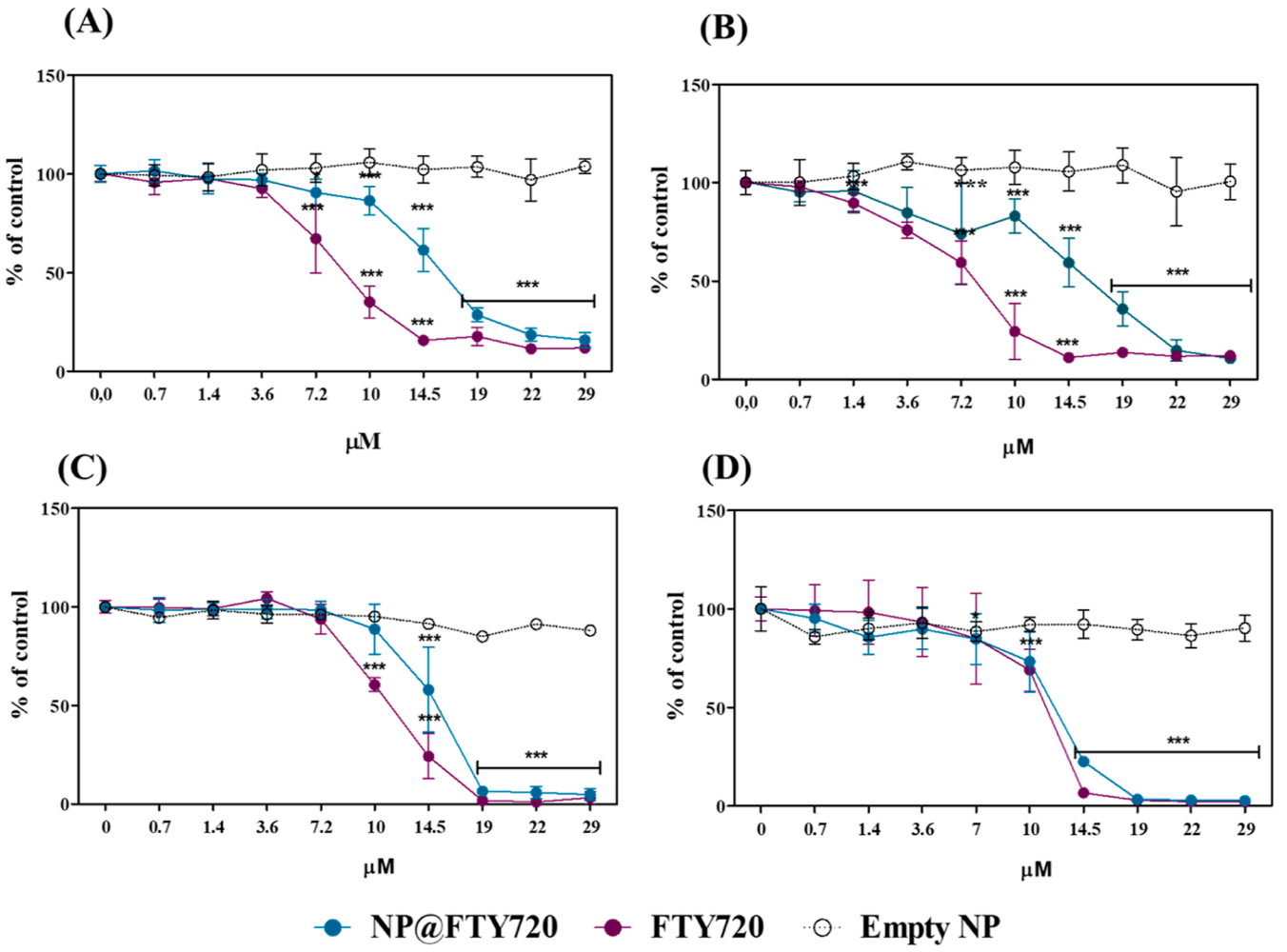

Figure 4. Cytotoxicity profile of FTY720, NP@FTY720, and empty NPs. (A) HepaRG cells after 24 h of incubation. (B) HepaRG cells after 48 h of incubation. (C) A549 cells after 24 h of incubation. (D) A549 cells after 48 h of incubation. Mean ± SD of three independent experiments in triplicate. Asterisks indicate a difference compared to the control (*P < 0.5 and ***P < 0.001).

The published data indicate that FTY720 decreases cell viability in a concentration-dependent manner, which is consistent with the results obtained in this study. Cytotoxicity investigations were also performed for different types of FTY720 NPs, including graphene oxide, liposomal, and calcium phosphate-based NPs.[21,22,50] As observed here, these authors also reported that cell viability decreased in a concentration-dependent manner upon incubation with FTY720 NPs.

Cell viability tests were also performed in VeroCCL81 cells, as these cells were used to study the antiviral activity of FTY720 and NP@FTY720 against SARS-CoV-2. In addition to 24 and 48 h, cells were incubated for 72 h following the viral infection protocol (Figure 5). As observed for human cells, FTY720 and NP@FTY720 induced a concentration-dependent reduction in cell viability in VeroCCL81 cells. Recently, Risner and co-workers described a similar result for VeroCCL81 incubated with FTY720 for 24 h.[51] Here, free FTY720 toxicity was approximately twofold higher than that of NP@FTY720 for VeroCCL81 cells after 24 and 48 h of incubation (Figure 5A,B). However, this difference was equalized after 72 h of incubation; thus, the values of IC_{50} after 72 h were 3.2 μM for free FTY720 and 5.2 μM for NP@FTY720 (Figure 5C). From these results, we concluded that concentrations below 1.4 μM of both free FTY720 and NP@FTY720 are non-cytotoxic to VeroCCL81 cells and are suitable for studying their antiviral activity against SARS-CoV-2.

3.4. NP@FTY720 Uptake in VeroCCL81. NP@FTY720-DiO internalization kinetics were performed in VeroCCL81 cells to investigate the minimum incubation period necessary for significant NP uptake. For this, cells were incubated with NPs for different time points and processed for flow cytometry. We observed that NP uptake significantly occurred 4 h after incubation, compared to controls (cells not exposed to NPs and cells exposed to non-fluorescent NPs) (Figure 6A). Based on these results, we designed further experiments to investigate the particle internalization mechanisms.

The mechanisms through which NP@FTY720-DiO are internalized by the cells were addressed by treating them with pharmacological inhibitors of different endocytic pathways before incubation for 4 h. As shown in Figure 6B, NP@FTY720-DiO was internalized by a combination of different uptake routes (caveolin, macropinocytosis, dynamin, and microtubule-mediated endocytosis). The results were indicated by the reduction in fluorescence intensity in VeroCCL81 cells upon pre-treatment with pharmacological inhibitors (nystatin, amiloride, hydroxy-dynasore, and nocodazole, respectively).

NP@FTY720-DiO uptake in cells pre-incubated with dynasore was nearly 80% lower than that in the control group (Figure 6B), indicating that dynamin is an essential

https://doi.org/10.1021/acsabm.2c00349
ACS Appl. Bio Mater. XXXX, XXX, XXX−XXX

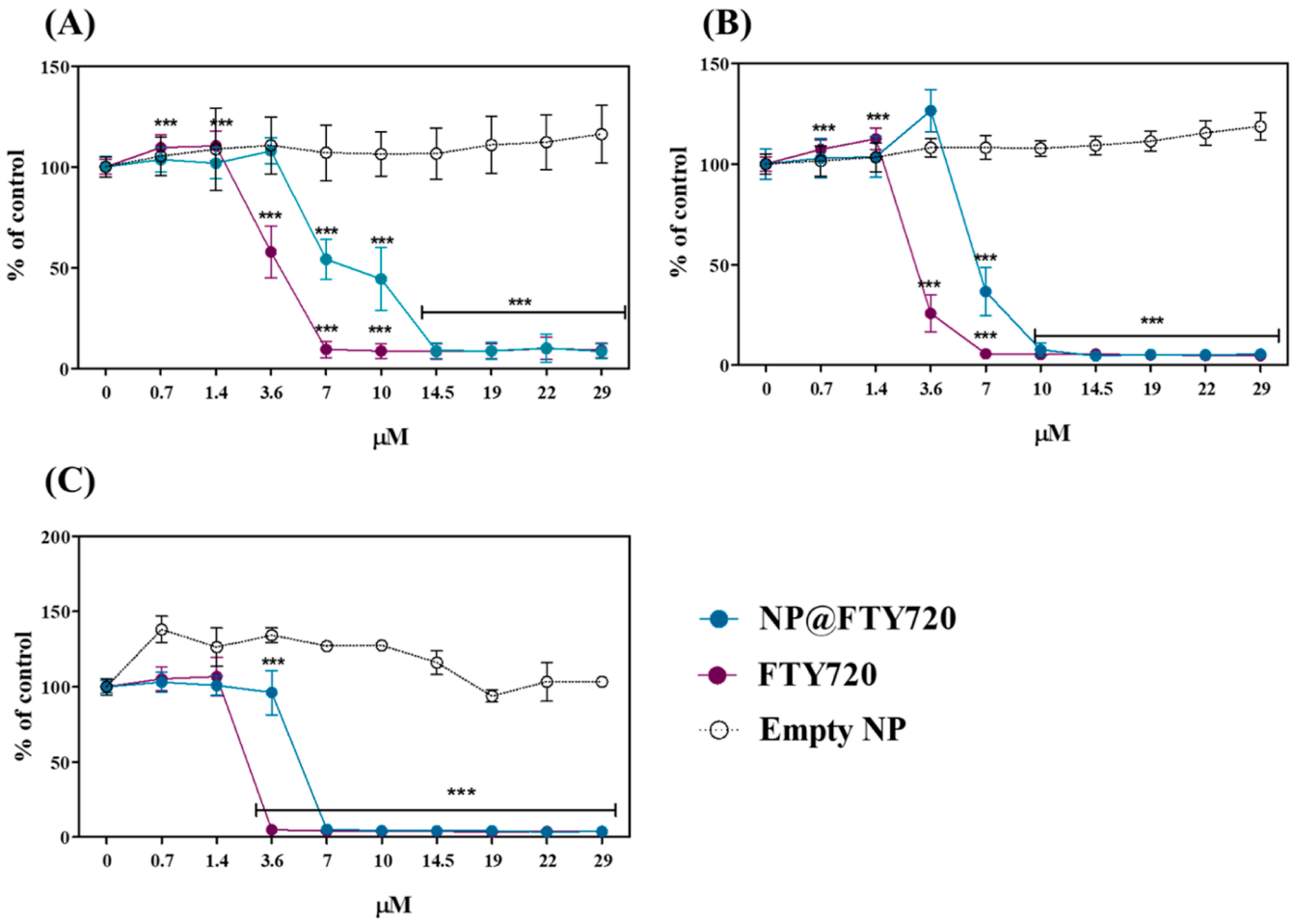

Figure 5. Cytotoxicity profiles of FTY720, NP@FTY720, and empty NPs in VeroCCL81 cells. (A) 24, (B) 48, and (C) 72 h. Mean ± SD of three independent experiments in triplicate. Asterisks indicate a difference compared to the control (*P < 0.5 and ***P < 0.001).

protein for NP@FTY720 internalization. This GTPase is one of the cell's main regulators of endocytosis because it is required for phagocytosis, clathrin- and caveolin-mediated endocytosis (CVME), as well as some clathrin- and caveolin-independent uptake pathways.[52] Thus, strong inhibition of the NP@FTY720-DiO intracellular concentration upon dynasore pre-treatment was expected.

Clathrin-mediated endocytosis is a dynamin-dependent process and one of the most representative uptake routes for 100−200 nm NPs.[53,54] However, pre-incubation of VeroCCL81 cells with cadaverine did not significantly reduce NP@FTY720-DiO uptake (Figure 6B), which suggests that the NP uptake mechanisms occurred mostly in a clathrin-independent manner. CVME is one of the best-characterized clathrin-independent and dynamin-dependent endocytosis pathways.[55,56] Here, pre-treatment with nystatin, an inhibitor of CVME, led to a significant reduction in NP@FTY720-DiO uptake (almost 40%) (Figure 6B). Although CVME is characterized as flask-shaped membrane invagination, approximately 50−80 nm in size,[57] it has already been reported that spherical PLGA NPs of 100−200 nm can be internalized via this endocytic route.[58−60] In these studies, the polymeric NPs were also internalized via clathrin-mediated endocytosis and/or macropinocytosis.

Macropinocytosis may also take place in the NP@FTY720-DiO uptake process, as the NP intracellular concentration significantly decreased (∼30%) in cells pre-treated with amiloride (Figure 6B). This internalization mechanism is clathrin-, caveolin-, and dynamin-independent and occurs via the formation of actin-driven membrane protrusions in a non-selective manner.[61,62] Due to its non-specificity and ability to engulf micron-sized particles, the macropinocytosis of polymeric NPs commonly occurs together with other types of uptake pathways, such as clathrin- and caveolin-mediated endocytosis.[59,63−65]

Since the drug release study indicated a pH dependence for FTY720 release from the NP, and MTT assays revealed that a cytotoxic effect occurs upon NP@FTY720 exposure, it is most likely that NP@FTY720-DiO is transported to acidic organelles upon cellular internalization, where drug release may occur. By confocal microscopy, we confirmed that after 4 h of incubation, NP@FTY720-DiO co-localizes with the LysoTracker-labeled lysosomes of VeroCCL81 cells, with a Pearson correlation coefficient (PCC) above 0.5 (Figure 6C); the co-localization of NP@FTY720-DiO and lysosomes can be seen as a yellow fluorescence signal in the merged image. This result reinforces that after cellular internalization, NP@FTY720-DiO follows the classical endocytic pathway in which endocytosed vesicles are transported to early and late endosomes and end up in the lysosomes.[66,67]

Taken together, the results obtained from the uptake assays indicated that NP@FTY720-DiO was actively internalized by VeroCCL81 cells mostly through a dynamin-dependent mechanism, of which CVME and macropinocytosis were the

https://doi.org/10.1021/acsabm.2c00349
ACS Appl. Bio Mater. XXXX, XXX, XXX−XXX

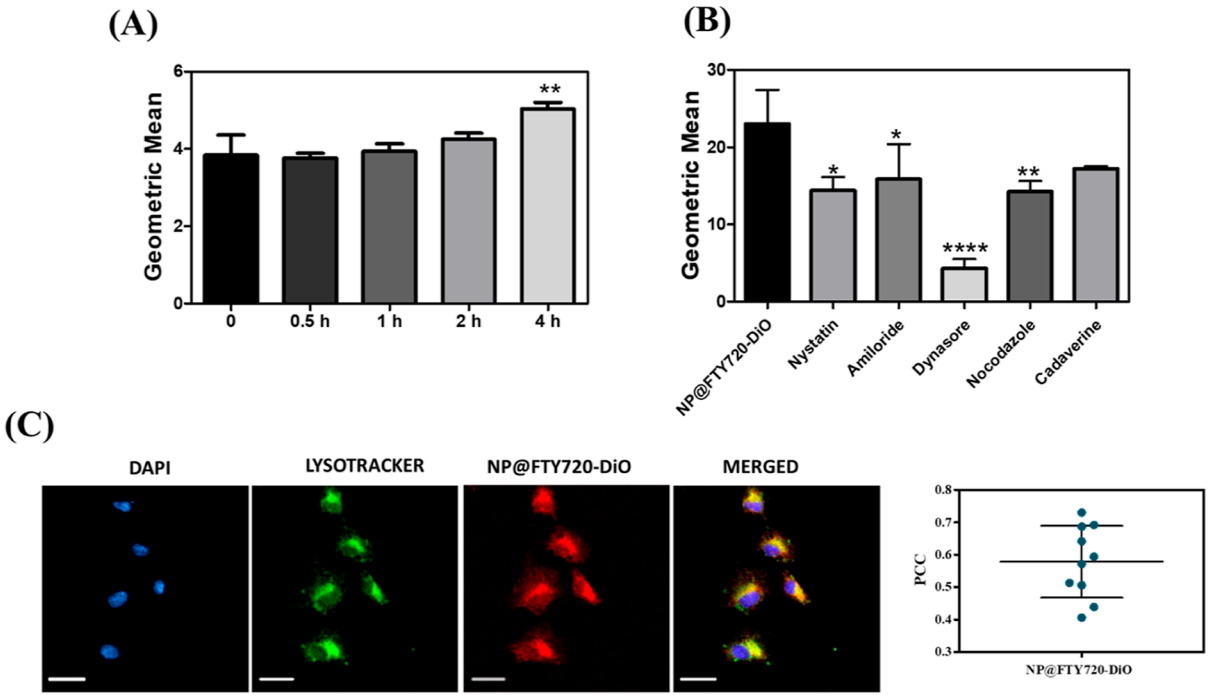

Figure 6. NP@FTY720-DiO internalization in VeroCCL81 cells. (A) Internalization kinetics of 5×10^9 particles/mL in VeroCCL81 cells. Cells were incubated for different time points and processed for flow cytometry by which the fluorescent intensity of NP@FTY720-DiO was acquired. The results express the geometric mean of the fluorescence intensity and represent the mean ± SD of three independent replicates. (B) VeroCCL81 cells were treated with different pharmacological endocytosis inhibitors before incubation with 5×10^9 particles/mL for 4 h in the presence of the inhibitors. The results express the geometric mean of the fluorescence intensity and represent the mean ± SD of three independent replicates. (C) Images acquired with a laser confocal microscope and PCC showing the intracellular co-localization of NP@FTY720-DiO with lysosomes after VeroCCL81 cells were incubated with 5×10^9 particles/mL for 4 h. Scale bar = 50 nm.

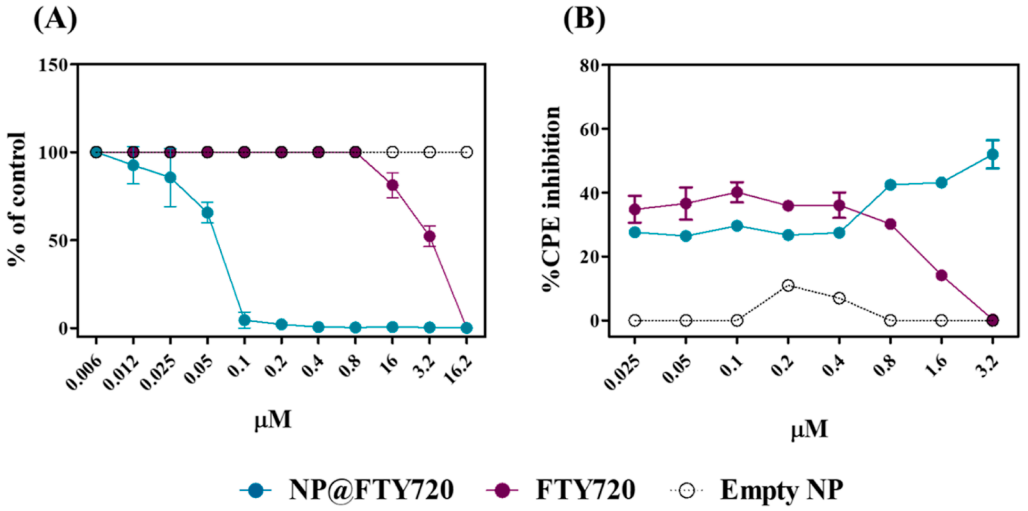

Figure 7. Antiviral activity of NP@FTY720. (A) Viral RNA production of SARS-CoV-2 in VeroCCL81 cells. The viral titers were quantified via RT-qPCR 72 h post-infection in the presence of serial twofold dilutions of FTY720, NP@FTY720, or empty NP. Individual data points represent means ± SD from four independent replicates in two biological experiments. (B) FTY720, NP@FTY720, or empty NP activity on CPE induced by SARS-CoV-2 in VeroCCL81 cells. CPE inhibition was assessed 72 h post-infection in the presence of serial twofold dilutions of FTY720, NP@FTY720, or empty NP, using CellTiter-Glo. Individual data points represent mean ± SD from three independent replicates in two biological experiments.

most representative uptake pathways. Furthermore, NP@FTY720 was transported to lysosomes, where FTY720 was rapidly released from the nanosystem in low-pH organelles, a fact previously evidenced *in vitro* release studies (Figure 3).

3.5. NP@FTY720 Antiviral SARS-CoV-2 Activity. In order to study the effect of FTY720, NP@FTY720, and empty NPs on the proliferation of SARS-CoV-2, RT-qPCR and CTG assays have been performed. Twofold serial dilutions of FTY720, NP@FTY720, or empty NPs were applied to infected VeroCCL81 cells to analyze the effect of NP@FTY720 on viral RNA (vRNA) and infectious virus production. While the IC_{50} value of FTY720 against the host cell line was found to be 5.3 μM (Figure 5C), the respective IC_{50} value of NP@FTY720 on the virus proliferation was

https://doi.org/10.1021/acsabm.2c00349
ACS Appl. Bio Mater. XXXX, XXX, XXX−XXX

determined to be about 100-times more potent (IC_{50} value = 0.05 μM) (Figure 7A) which clearly demonstrates the non-cytotoxic character of the nanoencapsulated drug. Furthermore, nanoencapsulation of FTY720 improved significantly (about 70-fold) the antiviral activity against SARS-CoV-2 as clearly shown by the IC_{50} value of 3.3 μM of FTY720 on the virus proliferation (Figure 7A). In the CTG inhibition assay, the incubation of cells with NP@FTY720 showed inhibition of infectious viral particle production >50% at non-cytotoxic levels (IC_{50} value = 0.7 μM), while FTY720 was not able to inhibit CPE below cytotoxic concentration levels (Figure 7B). These results demonstrate that SARS-CoV-2 vRNA production was substantially more sensitive to NP@FTY720, indicating its antiviral activity against SARS-CoV-2 with higher potency than free FTY720.

Moreover, empty NP did not influence vRNA synthesis or CPE, which demonstrated that the anti-SARS-CoV-2 activity observed for NP@FTY720 was induced by the combination of the drug and the developed nanosystem.

One of the advantages of NP drug delivery systems is the possibility to enhance drug pharmacokinetics and pharmacodynamics properties by modulating their solubility, drug release profile, diffusivity, and bioavailability.[68] In the case of FTY720, it has been shown that its entrapment into nanoparticulated systems results in better therapeutic efficacy and improved pharmacokinetic properties compared to free drugs.[21,69] For example, Mao et al. developed a liposomal FTY720 that increased its stability in aqueous media and prolonged circulation time in a mouse model compared to free FTY720.[21] A different study also showed that liposomal FTY720 NP had higher oral bioavailability *in vivo* and increased activity against leukemia cells than free FTY720.[69]

Here, we observed that nanoencapsulation was essential to increase the potency of FTY720 antiviral activity against SARS-CoV-2 below the cytotoxic concentration, as the IC_{50} value of NP@FTY720 to inhibit viral particle production was 70-fold lower than that observed for free FTY720. This result corroborates a recent study that showed that 5 μM of FTY720 can inhibit SARS-CoV-2 production in VeroCCL81 infected cells.[51] Although the exact mechanism through which FTY720 inhibits viral particle synthesis remains to be elucidated, we hypothesize that NPs may lead to an increase in its bioavailability and reduced degradation since FTY720 is sparingly soluble and unstable in aqueous buffers.[21] Consequently, even at low concentrations, NP@FTY720 achieved the desired effect.

Taken together, these results demonstrate the potential of NP@FTY720 to improve the biosafety and anti-SARS-CoV-2 activity of the drug. In addition to improving the therapeutic efficacy of drugs, NPs may also reduce adverse side effects.[68] This is particularly important for FTY720, since its administration is often associated with several side effects such as headache, fatigue, reduction in the heart rate at the first dose, macular edema, altered liver enzymes, and risk of skin cancer development.[70] Drug entrapment into polymeric nanosystems may offer a safer treatment option.

4. CONCLUSIONS

The present study was designed to evaluate the potential of the drug repurposing approach associated with nanotechnology for COVID-19 treatment. The development of a PLGA-based nanosystem for FTY720 represents an innovative strategy. The positively charged 150 nm-NP@FTY720 was stable for up to 3 months and displayed high drug encapsulation efficacy. The drug release study revealed that FTY720 release from PLGA NPs was pH-dependent because an acidic environment was necessary for drug release. Compared to the free drug, NP@FTY720 was less cytotoxic to both human and VeroCCL81 cell lines, which highlights the potential of nanoencapsulation for biosafety improvement. The nanosystems were actively endocytosed by VeroCCL81 cells, mainly via CVME and micropinocytosis, and co-localized with lysosomes, where drug release may occur. Furthermore, we showed that NP@FTY720 not only exhibited anti-SARS-CoV-2 activity at non-cytotoxic concentrations, but its biological potential for viral infection inhibition was nearly 70 times higher than the free drug potential. Additionally, the nanosystem reduced the CPE caused by the virus in VeroCCL81 cells.

Based on these results, we conclude that the entrapment of FTY720 into the PLGA nanosystem is essential for enhancing its biosafety and antiviral activity. Thus, NP@FTY720 is a possible future candidate for COVID-19 treatment. Further studies on the mechanism of action and tests in animal models are required to explore their therapeutic potential.

AUTHOR INFORMATION

Corresponding Author

Valtencir Zucolotto − *Nanomedicine and Nanotoxicology Group, Physics Institute of São Carlos, São Paulo University, 13566-590 São Carlos, São Paulo, Brazil;* orcid.org/0000-0003-4307-3077; Email: zuco@ifsc.usp.br

Authors

Renata Rank Miranda − *Nanomedicine and Nanotoxicology Group, Physics Institute of São Carlos, São Paulo University, 13566-590 São Carlos, São Paulo, Brazil;* orcid.org/0000-0001-8774-2418

Natália Noronha Ferreira − *Nanomedicine and Nanotoxicology Group, Physics Institute of São Carlos, São Paulo University, 13566-590 São Carlos, São Paulo, Brazil*

Edmarcia Elisa de Souza − *Unit for Drug Discovery, Department of Parasitology, Institute of Biomedical Sciences, University of Sao Paulo, 05508-000 Sao Paulo, Sao Paulo, Brazil*

Paula Maria Pincela Lins − *Nanomedicine and Nanotoxicology Group, Physics Institute of São Carlos, São Paulo University, 13566-590 São Carlos, São Paulo, Brazil;* orcid.org/0000-0002-8663-4463

Leonardo Miziara Barboza Ferreira − *Nanomedicine and Nanotoxicology Group, Physics Institute of São Carlos, São Paulo University, 13566-590 São Carlos, São Paulo, Brazil*

Arne Krüger − *Unit for Drug Discovery, Department of Parasitology, Institute of Biomedical Sciences, University of Sao Paulo, 05508-000 Sao Paulo, Sao Paulo, Brazil;* orcid.org/0000-0002-5531-9508

Valéria Maria de Oliveira Cardoso − *Nanomedicine and Nanotoxicology Group, Physics Institute of São Carlos, São Paulo University, 13566-590 São Carlos, São Paulo, Brazil*

Edison Luiz Durigon − *Unit for Drug Discovery, Department of Parasitology, Institute of Biomedical Sciences, University of Sao Paulo, 05508-000 Sao Paulo, Sao Paulo, Brazil;* Present Address: Department of Microbiology, Institute of Biomedical Sciences, University of São Paulo, 05508-000 São Paulo, São Paulo, Brazil

Carsten Wrenger − *Unit for Drug Discovery, Department of Parasitology, Institute of Biomedical Sciences, University of*

https://doi.org/10.1021/acsabm.2c00349
ACS Appl. Bio Mater. XXXX, XXX, XXX−XXX

Sao Paulo, 05508-000 Sao Paulo, Sao Paulo, Brazil;
orcid.org/0000-0001-5987-1749

Complete contact information is available at:
https://pubs.acs.org/10.1021/acsabm.2c00349

Author Contributions

R.R.M., N.N.F., and E.E.S. contributed equally to the study. R.R.M. and N.N.F.: conceptualization, methodology, data curation, writing, review, and editing. P.M.P.L., E.E.S., A.K., L.M.B.F., and V.M.d.O.C.: methodology, data curation, writing, review, and editing. E.L.D.: responsible for training the team in the BSL3 facility. C.W.: data curation, supervision, writing. V.Z.: conceptualization, data curation, supervision, funding acquisition, project administration, writing, review, and editing.

Notes

The authors declare no competing financial interest.

■ ACKNOWLEDGMENTS

The authors are grateful to Coordenação de Aperfeiçoamento de Pessoal de Nível Superior (Ref 88887.506832/2020-00) and Conselho Nacional de Desenvolvimento Científico e Tecnológico (CNPq, Brazil) as well as Fundação de Amparo à Pesquisa do Estado de São Paulo (FAPESP, Ref 2015/26722-8) for the financial assistance. This study is a part of project 88887.506832/2020-00. N.N.F., E.E.S., and A.K. received fellowships from FAPESP Refs 2019/25645-0, 2020/12277-0 and 2018/08820-0, respectively.

■ REFERENCES

(1) Zhu, N.; Zhang, D.; Wang, W.; Li, X.; Yang, B.; Song, J.; Zhao, X.; Huang, B.; Shi, W.; Lu, R.; Niu, P.; Zhan, F.; Ma, X.; Wang, D.; Xu, W.; Wu, G.; Gao, G. F.; Tan, W. A Novel Coronavirus from Patients with Pneumonia in China, 2019. *N. Engl. J. Med.* **2020**, *382*, 727−733.

(2) Vogel, A. C.; Schmidt, H.; Loud, S.; McBurney, R.; Mateen, F. J. Impact of the COVID-19 Pandemic on the Health Care of >1,000 People Living with Multiple Sclerosis: A Cross-Sectional Study. *Mult. Scler. Relat. Disord.* **2020**, *46*, 102512.

(3) Stefaniak, A. A.; Białynicki-Birula, R.; PiotrKrajewski, K.; Matusiak, Ł.; Mohamad Goldust, J. C. S. Itch in the era of COVID-19 pandemic: An unfolding scenario. *Dermatol. Ther.* **2020**, *3*, No. e13477.

(4) dos Santos, W. G. Impact of Virus Genetic Variability and Host Immunity for the Success of COVID-19 Vaccines. *Biomed. Pharmacother.* **2021**, *136*, 111272.

(5) Águas, R.; Mahdi, A.; Shretta, R.; Horby, P.; Landray, M.; White, L.; Arifi, F.; Zhumalieva, C.; Lubis, I. N. D.; Monteiro, A. B.; Moldokmatova, A.; Chen, S.; Estebesova, A.; Hussain, M.; Lata, D.; Bakare, E. A.; Getachew, B.; Sahak, M. N.; Chanthavilay, P.; Nji, A. M.; Aung, Y. N.; Hupert, N.; Tun, S. T. T.; Pan-Ngum, W.; Sarin, K. C.; Harsono, H.; Eybpoosh, S.; Coutinho, R. M.; Omoleke, S. A.; Nwosu, A. P.; Luangasanatip, N.; Kutmanova, A.; Dooronbekova, A.; Ximenes, A.; Monteiro, M.; Celhay, O.; Adib, K.; Salim, A. H.; Yunanda, Y.; Fariba, M. H.; Azzeri, A.; Hancock, P.; Bekrizadeh, H.; Saeedzai, S. A.; Alona, I.; Mzumara, G. W.; Martins, J.; Herrera-Diestra, J. L.; Sharifi, H.; Abdyldaev, T.; Jamshidi, B.; Hairi, N. N.; Nasir, N.; Zaman, R. U.; Obiesie, S.; Kraenkel, R. A.; Letchford, N.; Alves, L. R. F.; Adele, S.; Suárez-Idueta, L.; Advani, N.; Marzouk, M.; Mabombo, V.; Mukambetov, A.; Aderoba, A. K.; Tbalasubramaniam, B. L.; de Colombi, N. F.; Niha, M. A. V.; Obando, F.; Wattanasri, P.; Saralamba, S.; Shabaruddin, F.; Shimul, S. N.; Dahlui, M.; Naidoo, R.; Franco, C.; Klein, M. G.; Kubatova, A.; Jabin, N.; Kyaw, S. S.; Freitas, L. T.; Pokharel, S.; Ariana, P.; Mercado, C. E. G.; Ibragimov, S.; Medina, J. R. C.; Namedre, M. Potential Health and Economic Impacts of Dexamethasone Treatment for Patients with COVID-19. *Nat. Commun.* **2021**, *12*, 915−8.

(6) The Lancet. COVID-19: Learning as an Interdependent World. *Lancet* **2021**, *398*, 1105.

(7) Lazarus, J. V.; Ratzan, S. C.; Palayew, A.; Gostin, L. O.; Larson, H. J.; Rabin, K.; Kimball, S.; El-Mohandes, A. A Global Survey of Potential Acceptance of a COVID-19 Vaccine. *Nat. Med.* **2021**, *27*, 225−228.

(8) Valenzuela Nieto, G.; Jara, R.; Watterson, D.; Modhiran, N.; Amarilla, A. A.; Himelreichs, J.; Khromykh, A. A.; Salinas-Rebolledo, C.; Pinto, T.; Cheuquemilla, Y.; Margolles, Y.; López González Del Rey, N.; Miranda-Chacon, Z.; Cuevas, A.; Berking, A.; Deride, C.; González-Moraga, S.; Mancilla, H.; Maturana, D.; Langer, A.; Toledo, J. P.; Müller, A.; Uberti, B.; Krall, P.; Ehrenfeld, P.; Blesa, J.; Chana-Cuevas, P.; Rehren, G.; Schwefel, D.; Fernandez, L. Á.; Rojas-Fernandez, A. Potent Neutralization of Clinical Isolates of SARS-CoV-2 D614 and G614 Variants by a Monomeric, Sub-Nanomolar Affinity Nanobody. *Sci. Rep.* **2021**, *11*, 3318.

(9) Basu, D.; Chavda, V. P.; Mehta, A. A. Therapeutics for COVID-19 and Post COVID-19 Complications: An Update. *Curr. Res. Pharmacol. Drug Discov.* **2022**, *3*, 100086.

(10) Niknam, Z.; Jafari, A.; Golchin, A.; Danesh Pouya, F.; Nemati, M.; Rezaei-Tavirani, M.; Rasmi, Y. Potential Therapeutic Options for COVID-19: An Update on Current Evidence. *Eur. J. Med. Res.* **2022**, *27*, 6−15.

(11) Tao, K.; Tzou, P. L.; Nouhin, J.; Bonilla, H.; Jagannathan, P.; Shafer, R. W. SARS-CoV-2 Antiviral Therapy. *Clin. Microbiol. Rev.* **2021**, *34*, No. e0010921.

(12) Quan, J.; Zhang, X.; Ding, Y.; Li, S.; Qiu, Y.; Wang, R.; Zhou, X. Cucurbit[7]Uril as a Broad-Spectrum Antiviral Agent against Diverse RNA Viruses. *Virol. Sin.* **2021**, *36*, 1165−1176.

(13) Kwong, C. H. T.; Mu, J.; Li, S.; Fang, Y.; Liu, Q.; Zhang, X.; Kam, H.; Lee, S. M. Y.; Chen, Y.; Deng, F.; Zhou, X.; Wang, R. Reviving Chloroquine for Anti-SARS-CoV-2 Treatment with Cucurbit[7]Uril-Based Supramolecular Formulation. *Chin. Chem. Lett.* **2021**, *32*, 3019−3022.

(14) U.S. Food and Drug Administration. Coronavirus (COVID-19)|Drugs—COVID-19 Therapeutics. https://www.fda.gov/drugs/emergency-preparedness-drugs/coronavirus-covid-19-drugs (accessed 2022-05-31).

(15) Stasi, C.; Fallani, S.; Voller, F.; Silvestri, C. Treatment for COVID-19: An Overview. *Eur. J. Pharmacol.* **2020**, *889*, 173644.

(16) Singh, T. U.; Parida, S.; Lingaraju, M. C.; Kesavan, M.; Kumar, D.; Singh, R. K. Drug Repurposing Approach to Fight COVID-19. *Pharmacol. Rep.* **2020**, *72*, 1479−1508.

(17) Foerch, C.; Friedauer, L.; Bauer, B.; Wolf, T.; Adam, E. H. Severe COVID-19 Infection in a Patient with Multiple Sclerosis Treated with Fingolimod. *Mult. Scler. Relat. Disord.* **2020**, *42*, 102180.

(18) Amoruso, A.; Blonda, M.; D'Arrigo, G.; Grasso, R.; Di Francescantonio, V.; Verderio, C.; Avolio, C. Effect of Fingolimod Action on the Release of Monocyte-Derived Microvesicles in Multiple Sclerosis Patients. *J. Neuroimmunol.* **2018**, *323*, 43−48.

(19) Janneh, A. H.; Kassir, M. F.; Dwyer, C. J.; Chakraborty, P.; Pierce, J. S.; Flume, P. A.; Li, H.; Nadig, S. N.; Mehrotra, S.; Ogretmen, B. Alterations of Lipid Metabolism Provide Serologic Biomarkers for the Detection of Asymptomatic versus Symptomatic COVID-19 Patients. *Sci. Rep.* **2021**, *11*, 14232.

(20) Khalifa, S. A. M.; Yosri, N.; El-Mallah, M. F.; Ghonaim, R.; Guo, Z.; Musharraf, S. G.; Du, M.; Khatib, A.; Xiao, J.; Saeed, A.; El-Seedi, H. H. R.; Zhao, C.; Efferth, T.; El-Seedi, H. R. Screening for Natural and Derived Bio-Active Compounds in Preclinical and Clinical Studies: One of the Frontlines of Fighting the Coronaviruses Pandemic. *Phytomedicine* **2021**, *85*, 153311.

(21) Mao, Y.; Wang, J.; Zhao, Y.; Wu, Y.; Kwak, K. J.; Chen, C.-S.; Byrd, J. C.; Lee, R. J.; Phelps, M. A.; Lee, L. J.; Muthusamy, N. A Novel Liposomal Formulation of FTY720 (Fingolimod) for Promising Enhanced Targeted Delivery. *Nanomed. Nanotechnol. Biol. Med.* **2014**, *10*, 393−400.

(22) Masoudipour, E.; Kashanian, S.; Maleki, N.; Karamyan, A.; Omidfar, K. A Novel Intracellular PH-Responsive Formulation for FTY720 Based on PEGylated Graphene Oxide Nano-Sheets. *Drug Dev. Ind. Pharm.* **2018**, *44*, 99−108.
(23) Wang, Q.; Alshaker, H.; Böhler, T.; Srivats, S.; Chao, Y.; Cooper, C.; Pchejetski, D. Core Shell Lipid-Polymer Hybrid Nanoparticles with Combined Docetaxel and Molecular Targeted Therapy for the Treatment of Metastatic Prostate Cancer. *Sci. Rep.* **2017**, *7*, 5901.
(24) Rezaie Shirmard, L.; Bahari Javan, N.; Khoshayand, M. R.; Kebriaee-zadeh, A.; Dinarvand, R.; Dorkoosh, F. A. Nanoparticulate Fingolimod Delivery System Based on Biodegradable Poly (3-Hydroxybutyrate-Co-3-Hydroxyvalerate) (PHBV): Design, Optimization, Characterization and in-Vitro Evaluation. *Pharm. Dev. Technol.* **2017**, *22*, 860−870.
(25) Hasanzadeh, A.; Alamdaran, M.; Ahmadi, S.; Nourizadeh, H.; Bagherzadeh, M. A.; Mofazzal Jahromi, M. A.; Simon, P.; Karimi, M.; Hamblin, M. R. Nanotechnology against COVID-19: Immunization, Diagnostic and Therapeutic Studies. *J. Controlled Release* **2021**, *336*, 354−374.
(26) Cardoso, V. M. de O.; Moreira, B. J.; Comparetti, E. J.; Sampaio, I.; Ferreira, L. M. B.; Lins, P. M. P.; Zucolotto, V. Is Nanotechnology Helping in the Fight Against COVID-19? *Frontal Nanotechnol.* **2020**, *2*, 588915.
(27) Ferreira, N. N.; Granja, S.; Boni, F. I.; Prezotti, F. G.; Ferreira, L. M. B.; Cury, B. S. F.; Reis, R. M.; Baltazar, F.; Gremião, M. P. D. Modulating Chitosan-PLGA Nanoparticle Properties to Design a Co-Delivery Platform for Glioblastoma Therapy Intended for Nose-to-Brain Route. *Drug Delivery Transl. Res.* **2020**, *10*, 1729−1747.
(28) Ghediya, R. V.; Patel, M.; Pandya, D.; Shah, A. K.; Khunt, R. C. Stability Indicating Chromatographic Method Transfer of Immunomodulating Drug Fingolimod from High Performance Liquid Chromatography to New Generation Ultra Performance Liquid Chromatography with Comparative Validation Study. *J. Chem. Pharm. Res.* **2016**, *8*, 476−485.
(29) Ferreira, N. N.; Caetano, B. L.; Boni, F. I.; Sousa, F.; Magnani, M.; Sarmento, B.; Ferreira Cury, B. S.; Daflon Gremião, M. P. Alginate-Based Delivery Systems for Bevacizumab Local Therapy: In Vitro Structural Features and Release Properties. *J. Pharm. Sci.* **2019**, *108*, 1559−1568.
(30) Sardoiwala, M. N.; Karmakar, S.; Choudhury, S. R. Chitosan Nanocarrier for FTY720 Enhanced Delivery Retards Parkinson's Disease via PP2A-EzH2 Signaling in Vitro and Ex Vivo. *Carbohydr. Polym.* **2021**, *254*, 117435 June 2020.
(31) Araujo, D. B.; Machado, R. R. G.; Amgarten, D. E.; Malta, F. M.; de Araujo, G. G.; Monteiro, C. O.; Candido, E. D.; Soares, C. P.; de Menezes, F. G.; Santana, R. A. F.; Viana, A. O.; Dorlass, E.; Thomazelli, L.; Ferreira, L. C. S.; Botosso, V. F.; Carvalho, C. R. G.; Oliveira, D. B. L.; Pinho, J. R. R.; Durigon, E. L. SARS-CoV-2 Isolation from the First Reported Patients in Brazil and Establishment of a Coordinated Task Network. *Mem. Inst. Oswaldo Cruz* **2020**, *115*, No. e200342.
(32) Severson, W. E.; Shindo, N.; Sosa, M.; Fletcher, T., III; White, E. L.; Ananthan, S.; Jonsson, C. B. Development and Validation of a High-Throughput Screen for Inhibitors of SARS CoV and Its Application in Screening of a 100,000-Compound Library. *J. Biomol. Screen* **2007**, *12*, 33−40.
(33) Phillips, T.; Jenkinson, L.; McCrae, C.; Thong, B.; Unitt, J. Development of a High-Throughput Human Rhinovirus Infectivity Cell-Based Assay for Identifying Antiviral Compounds. *J. Virol. Methods* **2011**, *173*, 182−188.
(34) Corman, V. M.; Landt, O.; Kaiser, M.; Molenkamp, R.; Meijer, A.; Chu, D. K. W.; Bleicker, T.; Brünink, S.; Schneider, J.; Schmidt, M. L.; Mulders, D. G. J. C.; Haagmans, B. L.; van der Veer, B.; van den Brink, S.; Wijsman, L.; Goderski, G.; Romette, J.-L.; Ellis, J.; Zambon, M.; Peiris, M.; Goossens, H.; Reusken, C.; Koopmans, M. P. G.; Drosten, C. Detection of 2019 Novel Coronavirus (2019-NCoV) by Real-Time RT-PCR. *Euro Surveill.* **2020**, *25*, 2000045.
(35) Pushpakom, S.; Iorio, F.; Eyers, P. A.; Escott, K. J.; Hopper, S.; Wells, A.; Doig, A.; Guilliams, T.; Latimer, J.; McNamee, C.; Norris, A.; Sanseau, P.; Cavalla, D.; Pirmohamed, M. Drug Repurposing: Progress, Challenges and Recommendations. *Nat. Rev. Drug Discovery* **2018**, *18*, 41−58.
(36) Danhier, F.; Ansorena, E.; Silva, J. M.; Coco, R.; Le Breton, A.; Préat, V. PLGA-Based Nanoparticles: An Overview of Biomedical Applications. *J. Controlled Release* **2012**, *161*, 505−522.
(37) Han, S.; Cai, J.; Yang, J.; Zhang, J.; Wu, Q.; Zheng, W.; Shi, H.; Ajelli, M.; Zhou, X.-H.; Yu, H. Time-Varying Optimization of COVID-19 Vaccine Prioritization in the Context of Limited Vaccination Capacity. *Nat. Commun.* **2021**, *12*, 4673.
(38) Costa Clemens, S. A.; Clemens, C.; Folegatti, P. M.; Emary, K. R. W.; Weckx, L. Y.; Ratcliff, J.; Bibi, S.; Verena, A.; Mendes, D. A.; Milan, E. P.; Pittella, A.; Schwarzbold, A. V.; Sprinz, E.; Aley, P. K.; Bonsall, D.; Fraser, C.; Fuskova, M.; Gilbert, S. C.; Jenkin, D.; Kelly, S.; Kerridge, S.; Lambe, T.; Marchevsky, N. G.; Mujadidi, Y. F.; Plested, E.; Ramasamy, M. N.; Simmonds, P.; Golubchik, T.; Voysey, M.; Pollard, A. J. Efficacy of ChAdOx1 nCoV-19 (AZD1222) vaccine against SARS-CoV-2 lineages circulating in Brazil. *Nat. Commun.* **2021**, *12*, 5861.
(39) Zeraatpisheh, Z.; Mirzaei, E.; Nami, M.; Alipour, H.; Mahdavipour, M.; Sarkoohi, P.; Torabi, S.; Azari, H.; Aligholi, H. Local Delivery of Fingolimod through PLGA Nanoparticles and PuraMatrix-Embedded Neural Precursor Cells Promote Motor Function Recovery and Tissue Repair in Spinal Cord Injury. *Eur. J. Neurosci.* **2021**, *54*, 5620−5637.
(40) Langenbucher, F. Letters to the Editor: Linearization of Dissolution Rate Curves by the Weibull Distribution. *J. Pharm. Pharmacol.* **1972**, *24*, 979−981.
(41) Korsmeyer, R. W.; Gurny, R.; Doelker, E.; Buri, P.; Peppas, N. A. Mechanisms of Solute Release from Porous Hydrophilic Polymers. *Int. J. Pharm.* **1983**, *15*, 25−35.
(42) Peppas, N. A.; Narasimhan, B. Mathematical Models in Drug Delivery: How Modeling Has Shaped the Way We Design New Drug Delivery Systems. *J. Controlled Release* **2014**, *190*, 75−81.
(43) Weibull-1951-Paper3b.Pdf.
(44) Papadopoulou, V.; Kosmidis, K.; Vlachou, M.; Macheras, P. On the Use of the Weibull Function for the Discernment of Drug Release Mechanisms. *Int. J. Pharm.* **2006**, *309*, 44−50.
(45) Ferreira, N. N.; de Oliveira Junior, E.; Granja, S.; Boni, F. I.; Ferreira, L. M. B.; Cury, B. S. F.; Santos, L. C. R.; Reis, R. M.; Lima, E. M.; Baltazar, F.; Gremião, M. P. D. Nose-to-Brain Co-Delivery of Drugs for Glioblastoma Treatment Using Nanostructured System. *Int. J. Pharm.* **2021**, *603*, 120714.
(46) Pourtalebi Jahromi, L.; Ghazali, M.; Ashrafi, H.; Azadi, A. A Comparison of Models for the Analysis of the Kinetics of Drug Release from PLGA-Based Nanoparticles. *Heliyon* **2020**, *6*, No. e03451.
(47) Li, J.; Wang, S.-W.; Zhang, D.-S.; Sun, Y.; Zhu, C.-Y.; Fei, Q.; Hu, J.; Zhang, C.; Sun, Y.-M. FTY720-Induced Enhancement of Autophagy Protects Cells from FTY720 Cytotoxicity in Colorectal Cancer. *Oncol. Rep.* **2016**, *35*, 2833−2842.
(48) Marvaso, G.; Barone, A.; Amodio, N.; Raimondi, L.; Agosti, V.; Altomare, E.; Scotti, V.; Lombardi, A.; Bianco, R.; Bianco, C.; Caraglia, M.; Tassone, P.; Tagliaferri, P. Sphingosine Analog Fingolimod (FTY720) Increases Radiation Sensitivity of Human Breast Cancer Cells in Vitro. *Cancer Biol. Ther.* **2014**, *15*, 797−805.
(49) Rupp, T.; Pelouin, O.; Genest, L.; Legrand, C.; Froget, G.; Castagné, V. Therapeutic Potential of Fingolimod in Triple Negative Breast Cancer Preclinical Models. *Transl. Oncol.* **2021**, *14*, 100926.
(50) Wu, J.-Y.; Wang, Z.-x.; Zhang, G.; Lu, X.; Qiang, G.-H.; Hu, W.; Ji, A.-L.; Wu, J.-H.; Jiang, C.-P. Targeted Co-Delivery of Beclin I SiRNA and FTY720 to Hepatocellular Carcinoma by Calcium Phosphate Nanoparticles for Enhanced Anticancer Efficacy. *Int. J. Nanomed.* **2018**, *13*, 1265−1280.
(51) Risner, K. H.; Tieu, K. V.; Wang, Y.; Bakovic, A.; Alem, F.; Bhalla, N.; Nathan, S.; Conway, D. E.; Macklin, P.; Narayanan, A. Maraviroc Inhibits SARS-CoV-2 Multiplication and s-Protein

https://doi.org/10.1021/acsabm.2c00349
ACS Appl. Bio Mater. XXXX, XXX, XXX−XXX

Mediated Cell Fusion in Cell Culture. *bioRxiv* **2020**, DOI: 10.1101/2020.08.12.246389.
(52) Conner, S. D.; Schmid, S. L. Regulated Portals of Entry into the Cell. *Nature* **2003**, *422*, 37−44.
(53) Sousa De Almeida, M.; Susnik, E.; Drasler, B.; Taladriz-Blanco, P.; Petri-Fink, A.; Rothen-Rutishauser, B. Understanding Nanoparticle Endocytosis to Improve Targeting Strategies in Nanomedicine. *Chem. Soc. Rev.* **2021**, *50*, 5397−5434.
(54) Zhao, J.; Stenzel, M. H. Entry of Nanoparticles into Cells: The Importance of Nanoparticle Properties. *Polym. Chem.* **2018**, *9*, 259−272.
(55) Mayor, S.; Pagano, R. E. Pathways of Clathrin-Independent Endocytosis. *Nat. Rev. Mol. Cell Biol.* **2007**, *8*, 603−612.
(56) Sandvig, K.; Kavaliauskiene, S.; Skotland, T. Clathrin-Independent Endocytosis: An Increasing Degree of Complexity. *Histochem. Cell Biol.* **2018**, *150*, 107−118.
(57) Richter, T.; Floetenmeyer, M.; Ferguson, C.; Galea, J.; Goh, J.; Lindsay, M. R.; Morgan, G. P.; Marsh, B. J.; Parton, R. G. High-Resolution 3D Quantitative Analysis of Caveolar Ultrastructure and Caveola-Cytoskeleton Interactions. *Traffic* **2008**, *9*, 893−909.
(58) Zhang, J.; Chang, D.; Yang, Y.; Zhang, X.; Tao, W.; Jiang, L.; Liang, X.; Tsai, H.; Huang, L.; Mei, L. Systematic Investigation on the Intracellular Trafficking Network of Polymeric Nanoparticles. *Nanoscale* **2017**, *9*, 3269−3282.
(59) Sahin, A.; Esendagli, G.; Yerlikaya, F.; Caban-Toktas, S.; Yoyen-Ermis, D.; Horzum, U.; Aktas, Y.; Khan, M.; Couvreur, P.; Capan, Y. A Small Variation in Average Particle Size of PLGA Nanoparticles Prepared by Nanoprecipitation Leads to Considerable Change in Nanoparticles' Characteristics and Efficacy of Intracellular Delivery. *Artif. Cell Nanomed. Biotechnol.* **2017**, *45*, 1657−1664.
(60) Suen, W.-L. L.; Chau, Y. Size-Dependent Internalisation of Folate-Decorated Nanoparticles via the Pathways of Clathrin and Caveolae-Mediated Endocytosis in ARPE-19 Cells. *J. Pharm. Pharmacol.* **2014**, *66*, 564−573.
(61) Li, Y.-X.; Pang, H.-B. Macropinocytosis as a Cell Entry Route for Peptide-Functionalized and Bystander Nanoparticles. *J. Controlled Release* **2021**, *329*, 1222−1230.
(62) Hillaireau, H.; Couvreur, P. Nanocarriers' Entry into the Cell: Relevance to Drug Delivery. *Cell. Mol. Life Sci.* **2009**, *66*, 2873−2896.
(63) Tang, Z.-j.; Cao, Z.-m.; Guo, X.-w.; Chen, H.-j.; Lian, Y.; Zheng, W.-j.; Chen, Y.-j.; Lian, H.-z.; Hu, X. Cytotoxicity and Toxicoproteomic Analyses of Human Lung Epithelial Cells Exposed to Extracts of Atmospheric Particulate Matters on PTFE Fi Lters Using Acetone and Water. *Ecotoxicol. Environ. Saf.* **2020**, *191*, 110223.
(64) Tsolou, A.; Angelou, E.; Didaskalou, S.; Bikiaris, D.; Avgoustakis, K.; Agianian, B.; Koffa, M. D. Folate and Pegylated Aliphatic Polyester Nanoparticles for Targeted Anticancer Drug Delivery. *Int. J. Nanomed.* **2020**, *15*, 4899−4918.
(65) Nam, H. Y.; Kwon, S. M.; Chung, H.; Lee, S.-Y.; Kwon, S.-H.; Jeon, H.; Kim, Y.; Park, J. H.; Kim, J.; Her, S.; Oh, Y.-K.; Kwon, I. C.; Kim, K.; Jeong, S. Y. Cellular Uptake Mechanism and Intracellular Fate of Hydrophobically Modified Glycol Chitosan Nanoparticles. *J. Controlled Release* **2009**, *135*, 259−267.
(66) Wang, C.; Zhao, T.; Li, Y.; Huang, G.; White, M. A.; Gao, J. Investigation of Endosome and Lysosome Biology by Ultra PH-Sensitive Nanoprobes. *Adv. Drug Deliv. Rev.* **2017**, *113*, 87−96.
(67) Cullen, P. J.; Steinberg, F. To Degrade or Not to Degrade: Mechanisms and Significance of Endocytic Recycling. *Nat. Rev. Mol. Cell Biol.* **2018**, *19*, 679−696.
(68) Patra, J. K.; Das, G.; Fraceto, L. F.; Campos, E. V. R.; Rodriguez-Torres, M. D. P.; Acosta-Torres, L. S.; Diaz-Torres, L. A.; Grillo, R.; Swamy, M. K.; Sharma, S.; Habtemariam, S.; Shin, H.-S. Nano Based Drug Delivery Systems: Recent Developments and Future Prospects. *J. Nanobiotechnol.* **2018**, *16*, 71.
(69) De Mendoza, A. E.-H.; Castello-Cros, R.; Imbuluzqueta, E.; Cirauqui, C.; Pippa, R.; Odero, M. D.; Blanco-Prieto, M. J. Lipid Nanosystems Enhance the Bioavailability and the Therapeutic Efficacy of FTY720 in Acute Myeloid Leukemia. *J. Biomed. Nanotechnol.* **2015**, *11*, 691−701.
(70) Sharma, S.; Mathur, A. G.; Pradhan, S.; Singh, D. B.; Gupta, S. Fingolimod (FTY720): First Approved Oral Therapy for Multiple Sclerosis. *J. Pharmacol. Pharmacother.* **2011**, *2*, 49−51.

https://doi.org/10.1021/acsabm.2c00349
ACS Appl. Bio Mater. XXXX, XXX, XXX−XXX